indicates that a full structure refinement based upon a composite modulated structure approach is needed in order to obtain chemically plausible AMF's – in particular the chemically implausible spike associated with the $\mathbf{b}_Q$ axis shifts of the Q sub-structure anions and the $\mathbf{c}_H$ axis shifts of the H sub-structure should be refined.

References

ABAOUZ, A. (1988). PhD thesis, Univ. of Limoges, France.
BEVAN, D. J. M. & MANN, A. W. (1975). *Acta Cryst.* **B31**, 1406–1411.
BEVAN, D. J. M., MOHYLA, J., HOSKINS, B. F. & STEEN, R. J. (1990). *Eur. J. Solid State Inorg. Chem.* **27**, 451–465.
BRADLEY, C. J. & CRACKNELL, A. P. (1972). *The Mathematical Theory of Symmetry in Solids.* Oxford: Clarendon Press.
HYDE, B. G. & ANDERSSON, S. (1989). *Inorganic Crystal Structures.* New York: Wiley.
JANNER, A. & JANSSEN, T. (1980). *Acta Cryst.* **A36**, 408–415.
JUNG, W. & JUZA, R. (1973). *Z. Anorg. Allg. Chem.* **399**, 129–147.
MAKOVICKY, E. & HYDE, B. G. (1981). *Struct. Bonding*, **46**, 101–176.
MAKOVICKY, E. & HYDE, B. G. (1992). *Non-Commensurate Layered Structures*, edited by A. MEERSCHAUT, pp. 1–100. Switzerland: Trans Tech Publications.
MANN, A. W. & BEVAN, D. J. M. (1972). *J. Solid State Chem.* **5**, 410–418.
PÉREZ-MATO, J. M. (1991). *Methods of Structural Analysis of Modulated Structures and Quasi-crystals*, edited by J. M. PÉREZ-MATO, F. J. ZÚÑIGA & G. MADARIAGA, pp. 117–128. Singapore: World Scientific.
PÉREZ-MATO, J. M., MADARIAGA, G., ZÚÑIGA, F. J. & GARCIA ARRIBAS, A. (1987). *Acta Cryst.* **A43**, 216–226.
SMAALEN, S. VAN (1989). *J. Phys. Conden. Matter*, **1**, 2791–2800.
SMAALEN, S. VAN (1991*a*). *J. Phys. Conden. Matter*, **3**, 1247–1263.
SMAALEN, S. VAN (1991*b*). *Phys. Rev. B*, **43**, 11330–11341.
SMAALEN, S. VAN (1992). *Non-Commensurate Layered Structures*, edited by A. MEERSCHAUT, pp. 173–222. Switzerland: Trans Tech Publications.
THOMPSON, J. G., WITHERS, R. L., SELLAR, J., BARLOW, P. J. & HYDE, B. G. (1990). *J. Solid State Chem.* **88**, 465–475.
WITHERS, R. L., THOMPSON, J. G. & HYDE, B. G. (1991). *Acta Cryst.* **B47**, 166–174.
WOLFF, P. M. DE (1974). *Acta Cryst.* **A30**, 777–785.
WOLFF, P. M. DE (1988). *Z. Kristallogr.* **185**, 67.
WOLFF, P. M. DE, JANSSEN, T. & JANNER, A. (1981). *Acta Cryst.* **A37**, 625–636.

Acta Cryst. (1993). **B49**, 951–958

Two High-Pressure Tungsten Oxide Structures of W_3O_8 Stoichiometry Deduced from High-Resolution Electron Microscopy Images

BY M. SUNDBERG

Department of Inorganic Chemistry, Arrhenius Laboratory, Stockholm University, S-10691 Stockholm, Sweden

N. D. ZAKHAROV, I. P. ZIBROV, YU. A. BARABANENKOV

Institute of Crystallography, Russian Academy of Sciences, 117333 Moscow, Russia

V. P. FILONENKO

Institute of High Pressure Physics, Russian Academy of Sciences, Troitsk, 149092 Moscow Region, Russia

AND P. WERNER

Max-Planck-Institut für Mikrostrukturphysik, Weinberg 2, O-4050 Halle/Saale, Germany

(*Received* 18 *March* 1993; *accepted* 7 *June* 1993)

Abstract

Two new high-pressure tungsten oxides, prepared at $P = 50 \times 10^5$ kPa and $T = 1773$ K, have been investigated by high-resolution electron microscopy. The formula, W_3O_8 for both phases, and the structures were deduced from the micrographs and verified by simulated image calculations. The phases are both orthorhombic, with the following unit-cell dimensions determined from X-ray powder patterns: W_3O_8(I), $a = 6.386$ (9), $b = 10.43$ (5), $c = 3.80$ (1) Å, $V = 253.1$ Å^3, $Z = 2$, space group $C222$; W_3O_8(II), $a = 10.35$ (5), $b = 13.99$ (5), $c = 3.78$ (1) Å, $V = 547.3$ Å^3, $Z = 4$, space group $Pbam$. The first structure, W_3O_8(I), which is more dense than the other, is isostructural with U_3O_8 [Andresen (1958). *Acta Cryst.* **11**, 612–614] and with the high-pressure modification of Nb_3O_7F. The less densely packed phase, W_3O_8(II), has a new type of structure, which contains groups of four edge-sharing WO_6 octahedra

mutually linked by corner-sharing with single octahedra. Intergrowth between the two phases has been observed, and possible models of the intergrowth structure are given.

Introduction

Products obtained by reduction of tungsten trioxide have been extensively investigated both by X-ray diffraction and electron microscopy techniques. For most of the studies samples of known compositions were prepared by heating appropriate mixtures of W and WO_3 or WO_2 and WO_3 in sealed evacuated silica tubes at high temperatures.

Four structure types have been reported for WO_x within the $3 \geq x \geq 2.6$ region: {102} crystallographic shear (CS) structures ($3 > x > 2.93$) (Tilley, 1970; Sundberg & Tilley, 1974), {103} CS structures, of which $W_{20}O_{58}$ was the first representative ($2.93 > x > 2.88$) (Magnéli, 1950; Tilley, 1978–1979; Sundberg, 1981; Sahle, 1983), $W_{12}O_{34}$ ($x \simeq 2.83$) (Sundberg, 1978–1979) and $W_{18}O_{49}$ ($x = 2.72$) (Magnéli, 1949). The CS structures form two homologous series of phases with the general formulas W_nO_{3n-1} and W_nO_{3n-2} (Magnéli, 1953). Both structure types consist of slabs of corner-sharing WO_6 octahedra (ReO_3 type), which have an infinite extension in two dimensions and a characteristic width (n) in a third direction. In the {102} CS structures the slabs are mutually linked so that groups of four edge-sharing WO_6 octahedra are formed along {102} planes, while for the {103} CS phases groups of six edge-sharing octahedra are formed along {103} planes. The CS phases are often highly disordered. $W_{12}O_{34}$ and $W_{18}O_{49}$ form unique structures built up of WO_6 octahedra and WO_7 pentagonal bipyramids.

A couple of years ago, an investigation of the reduction of WO_3 and the formation of reduced WO_x phases at high temperature in combination with high pressure was started at the Institute of High-Pressure Physics in Troitsk. Some new WO_x phases were observed by a combination of X-ray diffraction and high-resolution electron microscopy (HREM) techniques (Barabanenkov, Zakharov, Zibrov, Filonenko & Werner, 1992; Barabanenkov, Valkovskii, Zakharov, Zibrov, Popov & Filonenko, 1992). The present study reports two further structures which were deduced from HREM images and verified by simulated-image calculations.

Experimental

The sample examined was prepared by partial reduction of WO_3 with carbon at high temperature in combination with high pressure. The reaction occurred between the graphite container material and a pressed tablet of WO_3 in a closed system (T = 1773 K, $P = 50 \times 10^5$ kPa). A detailed description of the experimental set-up and conditions will be presented elsewhere. The product obtained was a mass containing minute dark-red crystallites. The colour suggested that considerable reduction had taken place.

X-ray analysis was carried out with an X-ray powder diffractometer HZG-4, using Ni-filtered Cu $K\alpha$ radiation ($\lambda = 1.5418$ Å).* A thermogravimetry unit (Q-1500D) was used for analysis of the reaction product.

The electron microscopy specimen was prepared by crushing a small amount of the sample in an agate mortar. The fine powder was then dispersed in acetone (or n-butanol). A drop of the resulting suspension was put on a holey carbon film supported by a Cu grid. A JEOL JEM 4000EX transmission electron microscope in Halle was used to record the HREM images. The microscope was operated at an accelerating voltage of 400 kV. The radius (r) of the objective aperture used corresponded to 0.91 $Å^{-1}$ in reciprocal space and was larger than that (r_{Sch} = 0.62 $Å^{-1}$) which corresponded to the Scherzer resolution.

Crystallographic image processing (CIP) by the computer program system *CRISP* (Hovmöller, 1992) was applied to the HREM images. The computer-calculated diffraction pattern extended out to about 2 Å resolution. CIP gave similar results for 0.62 and 0.91 $Å^{-1}$ resolution, since the very high resolution reflections were very weak. The heavy-metal (tungsten) atom positions were obtained from the processed image, while the O atoms were all introduced into the structure models by consideration of available space, coordination and interatomic (W—W, W—O, O—O) distances. Simulated images of the deduced structure models were calculated with a local version of the *SHRLI* suite of programs (O'Keefe, Buseck & Iijima, 1978).

Results

X-ray powder diffraction and electron microscopy investigations of the specimens revealed the presence of two new WO_x phases, which will be denoted by (I) and (II). Unit-cell dimensions determined from the X-ray powder patterns are given in Table 1 and Table 2. The fact that both phases have a short c axis ($\simeq$ 3.8 Å) and another axis $\simeq$ 10.4 Å makes an intergrowth between the two structures very likely. The micrograph in Fig. 1 clearly illustrates that this actually seems to be the case, as phase (I) in the middle is linked to phase (II) on both sides without

* Refinements of the two structures W_3O_8(I) and W_3O_8(II) by profile analysis of a two-phase powder diffraction pattern are in progress (Sundberg, Werner, Zibrov & Louër, 1994).

Table 1. *Atomic coordinates of the* W_3O_8(I) *structure*

$a = 6.386$ (9), $b = 10.43$ (5), $c = 3.80$ (1) Å ($V = 253.1$ Å^3), space group *C*222, $Z = 2$. Probable error in the O position ± 0.05–0.1 Å.

	Point position	x	y	z
W1	2(*a*)	0	0	0
W2	4(*g*)	0	0.324 (4)	0
O1	2(*b*)	0	$\frac{1}{2}$	0
O2	2(*d*)	0	0	$\frac{1}{2}$
O3	4(*h*)	0	0.302	$\frac{1}{2}$
O4	8(*l*)	0.157	0.152	0.150

Table 2. *Atomic coordinates of the* W_3O_8(II) *structure*

$a = 10.35$ (5), $b = 13.99$ (5), $c = 3.78$ (1) Å ($V = 547.3$ Å^3), space group *Pbam*, $Z = 4$. Probable error in the O position ± 0.05–0.1 Å.

	Point position	x	y	z
W1	4(*c*)	0.030 (4)	0.388 (3)	0
W2	4(*c*)	0.215 (4)	0.087 (3)	0
W3	4(*c*)	0.374 (4)	0.333 (3)	0
O1	4(*c*)	0.045	0.165	0
O2	4(*c*)	0.130	$\frac{1}{2}$	0
O3	4(*c*)	0.192	0.320	0
O4	4(*c*)	0.343	0.185	0
O5	4(*c*)	0.386	0.470	0
O6	4(*c*)	0.027	0.388	$\frac{1}{2}$
O7	4(*c*)	0.215	0.087	$\frac{1}{2}$
O8	4(*c*)	0.374	0.333	$\frac{1}{2}$

much distortion of the structures. Fig. 1 also shows twinning of phase (I). The twin boundary is marked by arrows.

Phase (I)

Fig. 2(*a*) presents the HREM image of phase (I) with the corresponding electron diffraction (ED) pattern ([001] zone) inserted. The ED pattern shows systematic absence for *hk*0 reflections when $h + k = 2n + 1$. This is in agreement with the X-ray powder data which showed only reflections *hkl* with $h + k = 2n + 1$ to be systematically absent. Thus, possible space groups were *C*222, *Cmm*2, *C*2*mm* and *Cmmm*. In the micrograph a pseudohexagonal arrangement of black spots can be seen. The black contrast can be interpreted as projected metal (tungsten) atoms. Along the *b* axis, a threefold repetition of black spots, all on straight lines, can be discerned. This feature is more obvious in the density map in Fig. 2(*b*) after applying crystallographic image processing (CIP) to Fig. 2(*a*). By CIP, the plane-group symmetries $p21$, $p222$, $p22_12$, $p22_12_1$ and $c222$ were tested (Hovmöller, 1992). A very slight preference for the $c222$ plane group was obtained. From the black contrast features in the HREM image a structure model was deduced (Fig. 2*c*). The W-atom positions were determined from the processed image, and the O-atom positions (Table 1) were located in the model by consideration of interatomic (W—O) and (O—O) distances. In the suggested structure model the shortest W—W distance is 3.4 Å, and the W—O distances are in the range 1.85–2.6Å. The framework of polyhedra corresponds to the stochiometry W_3O_8. The space group *C*222 was finally assumed, as reasonable interatomic W—O and O—O distances could be obtained by using this symmetry. However, it was not possible to verify the symmetry by convergent-beam electron diffraction, because of domain intergrowth of the two W_3O_8 phases. Simulated images of the W_3O_8(I) structure model were calculated at different crystal thicknesses and defocus values. Some images are shown in Fig. 2(*d*). There is good agreement between the experimental image and the calculated one inserted in Fig. 2(*a*), which supports the interpretation of the deduced model.

The W_3O_8(I) structure is built up of WO_6 octahedra and WO_7 pentagonal bipyramids which share edges and corners in the (001) plane. Along the *a* axis the WO_7 pentagonal bipyramids are linked by edges to form pleated chains of edge-sharing WO_7 pentagonal bipyramids. The chains are mutually connected along the *b* axis by corner-sharing and by additional WO_6 octahedra.

The structure is isotypic with that of U_3O_8 according to Andresen (1958) and the high-pressure (Hp) modification of Nb_3O_7F (Hp-Nb_3O_7F) (Jahnberg, 1971). The unit-cell dimensions of the latter, $a = 6.475$ (1), $b = 10.514$ (1) and $c = 3.922$ (1) Å, are similar to those given in Table 1 of W_3O_8(I). Simulated-image calculations of the U_3O_8 structure suggested by Andresen (1958) and the U_3O_8 model proposed by Loopstra (1964) clearly showed that it was possible to distinguish between the two U_3O_8 structures from the contrast in the HREM images at

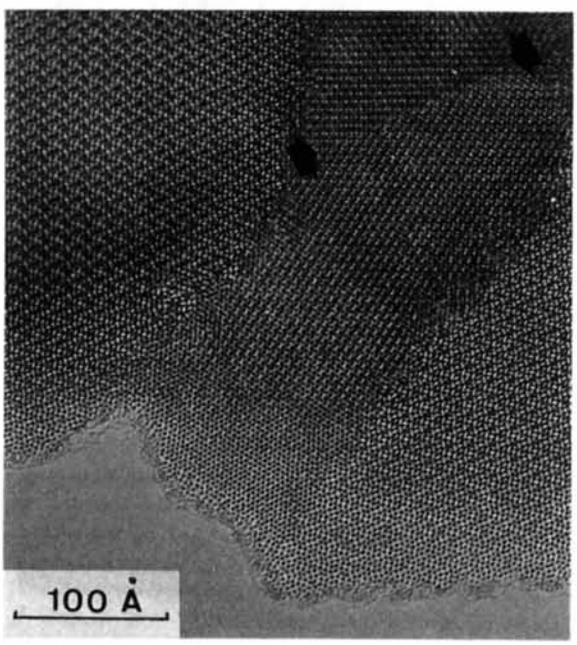

Fig. 1. Low-magnification micrograph showing intergrowth of W_3O_8(I) (middle part) and W_3O_8(II) (left and right parts). A twin plane in the W_3O_8(I) structure is illustrated by arrows.

some defocus values. The simulated images of the W_3O_8 structure, shown in Fig. 2(*d*), were very similar to those obtained of the U_3O_8 structure according to Andresen. The W_3O_8 formulá ($WO_{2.667}$) fits rather well with the value $WO_{2.59 \pm x}$, $x \simeq 0.05$–0.1, obtained from the gravimetric analysis of the sample.

Phase (II)

Fig. 3(*a*) shows an HREM image of phase (II) with a corresponding ED pattern inserted. The micrograph was recorded under the same conditions as above (phase I), which means that the black spots

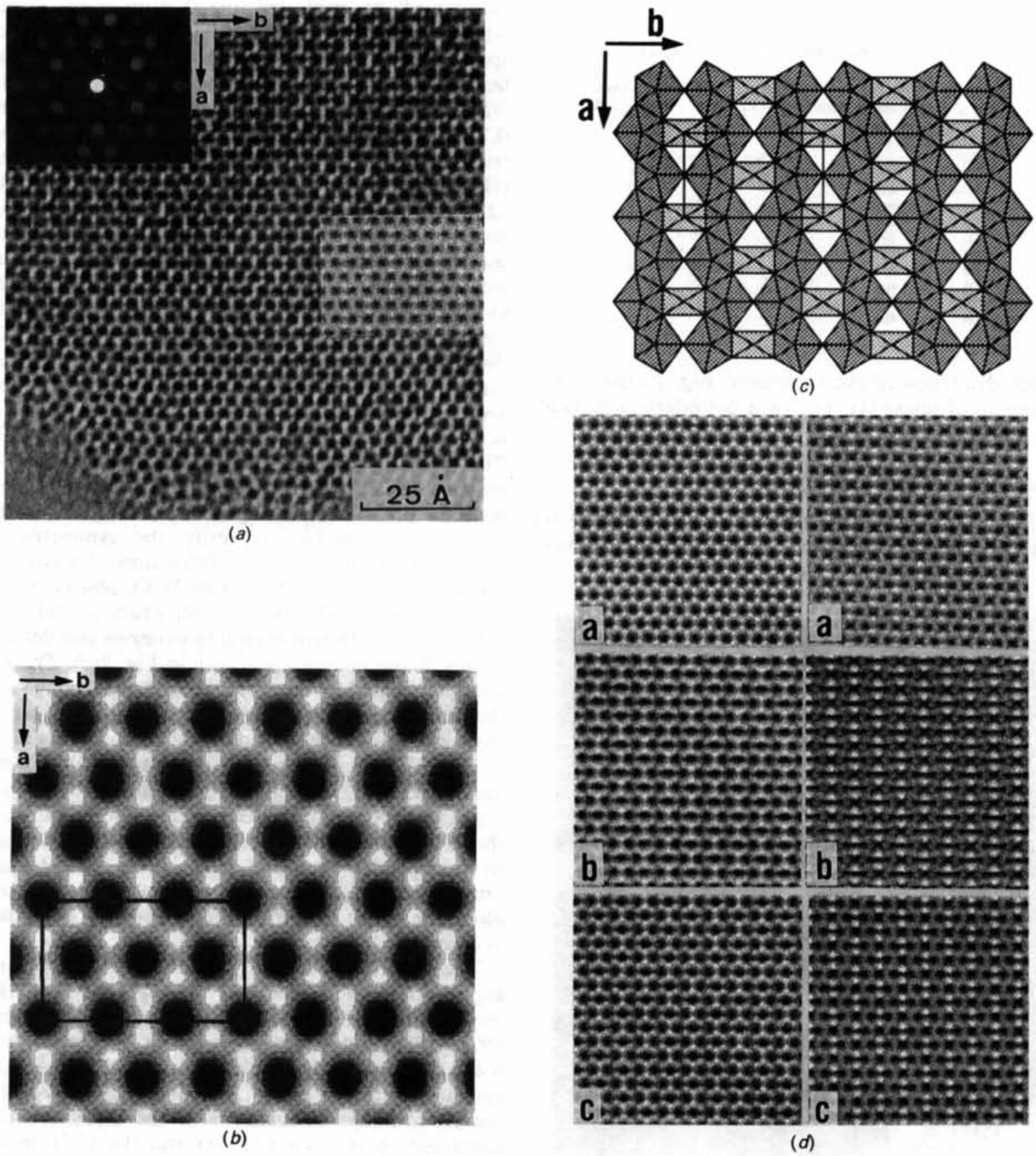

Fig. 2. The structure of W_3O_8(I). (*a*) HREM image ([001] zone) with the corresponding ED pattern and the simulated image (crystal thickness 19 Å, defocus value −380 Å) inserted; (*b*) the image processed by the CIP program; (*c*) deduced structure model; (*d*) some simulated images: crystal thickness *a* 19, *b* 38, *c* 57 Å; defocus values −300 Å (left), −400 Å (right).

can be interpreted as representing projected W atoms. The W-atom positions were deduced from the processed image in Fig. 3(*b*) after applying CIP to the HREM micrograph in Fig. 3(*a*). By the *CRISP* program the following plane-group symmetries were tested; *p*21, *p*222, $p22_12$ and $p22_12_1$. The best phase residual value (Hovmöller, 1992) was calculated for the $p22_12_1$ plane-group symmetry. Calculations of interatomic W—W distances showed the presence of two rather short ~3.2 Å distances. This distance indicates edge-sharing of WO_6 octahedra according to previous results obtained from single-crystal X-ray data studies of the $W_{20}O_{58}$ and $W_{25}O_{73}$ {103} CS structures (Magnéli, 1950; Sundberg, 1976). The structure model shown in Fig. 3(*c*) was deduced from the pattern of black spots in Fig. 3(*a*) in combination

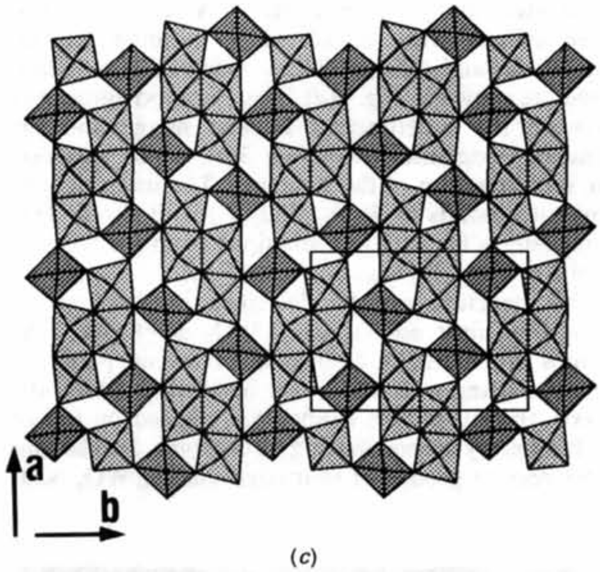

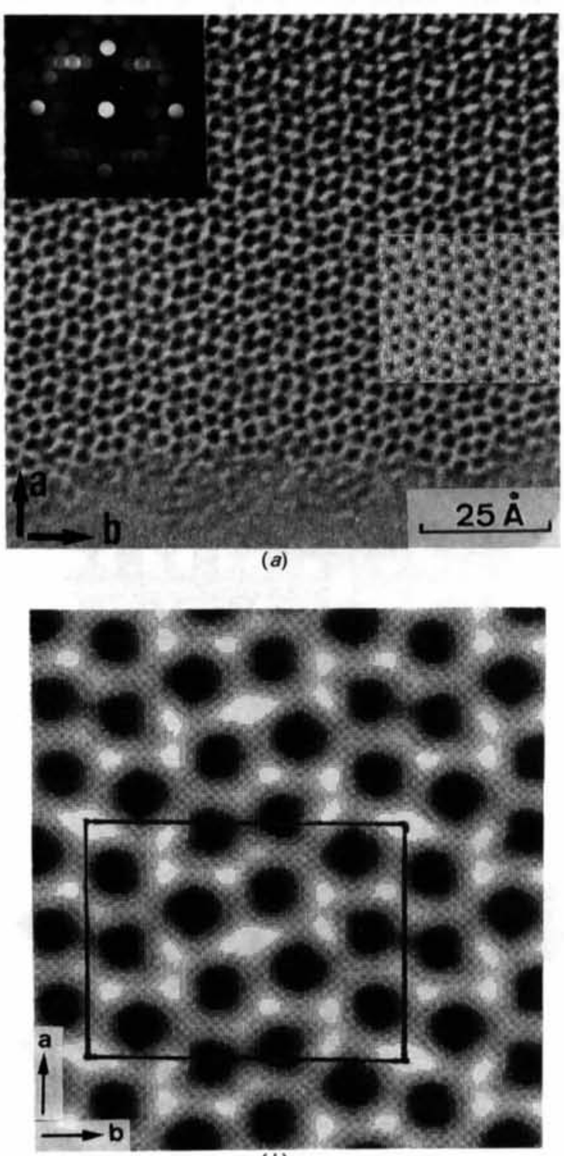

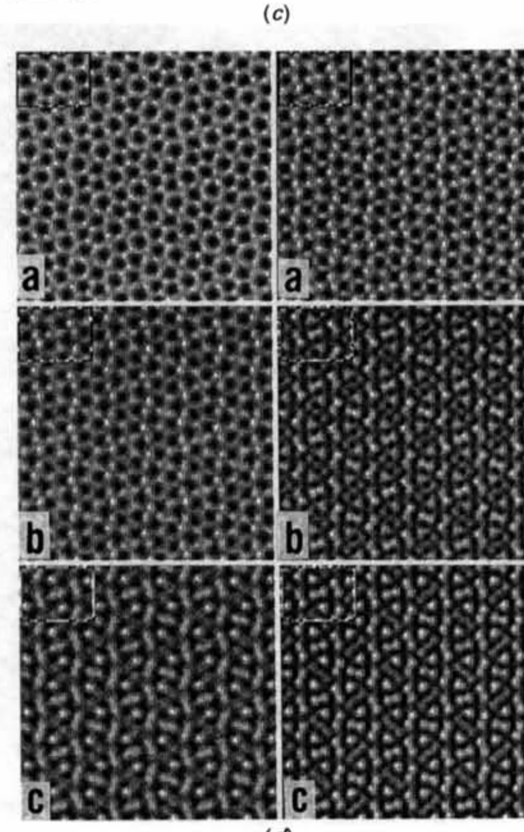

Fig. 3. The structure of W_3O_8(II). (*a*) HREM image ([001] zone) with the corresponding ED pattern and the simulated image (crystal thickness 19 Å, defocus value −380 Å) inserted; (*b*) the processed micrograph in (*a*); (*c*) deduced structure model; (*d*) some simulated images: crystal thickness *a* 19, *b* 38, *c* 57 Å; defocus values −300 Å (left), −400 Å (right).

with known interatomic W—W distances. The O atoms were located from considerations of available space and reasonable O-atom positions found by calculation of interatomic W—O and O—O distances. The *Pmab* space group was used. The W—O distances are all in the range 1.8–2.3 Å. The atomic parameters are given in Table 2. A series of simulated images were calculated at different crystal thicknesses and defocus values. A few of those simulated are shown in Fig. 3(*d*). There is good agreement between the experimental HREM image and the simulated one inserted in Fig. 3(*a*), which supports the interpretation of the structure. The unit-cell content corresponds to W_3O_8 ($WO_{2.667}$) with $Z = 4$. This composition fits with that obtained from the analysis of the product $WO_{2.59\pm x}$, $x \simeq 0.05$–0.1.

The structure can be described as built up of groups of four edge-sharing WO_6 octahedra. The groups are mutually connected in the *ab* plane by corner-sharing with additional octahedra. Along the *c* axis, the layers thus formed are stacked on top of each other by corner-sharing of O atoms. Similar but more regular groups of four edge-sharing WO_6 octahedra have previously been observed as structural building units in the {102} CS structures of WO_{3-x}, $0 < x < 0.07$ (Tilley, 1970; Sundberg & Tilley, 1974).

Intergrowth

The HREM image in Fig. 4(*a*) clearly illustrates that the two phases W_3O_8(I) (left) and W_3O_8(II) (right) are mutually connected. In the direction marked by an arrow, the black spots are closer to each other below the intergrowth boundary than above. This fact might indicate that the two structures transform into each other by small metal and oxygen atom displacements. Figs. 4(*b*) and 4(*c*) illustrate two possible models of the intergrowth boundary. In Fig. 4(*b*) the *bc* plane in the W_3O_8(I) structure is linked to the *ac* plane in the W_3O_8(II) structure. This latter is a possible model for the intergrowth of the two phases in the upper part of Fig. 1. In Fig. 4(*c*) the W_3O_8(I) structure, in twin orientation compared to Fig. 4(*b*), is connected to the W_3O_8(II) structure. This model illustrates a probable linkage of the two phases in Fig. 4(*a*). From the idealized

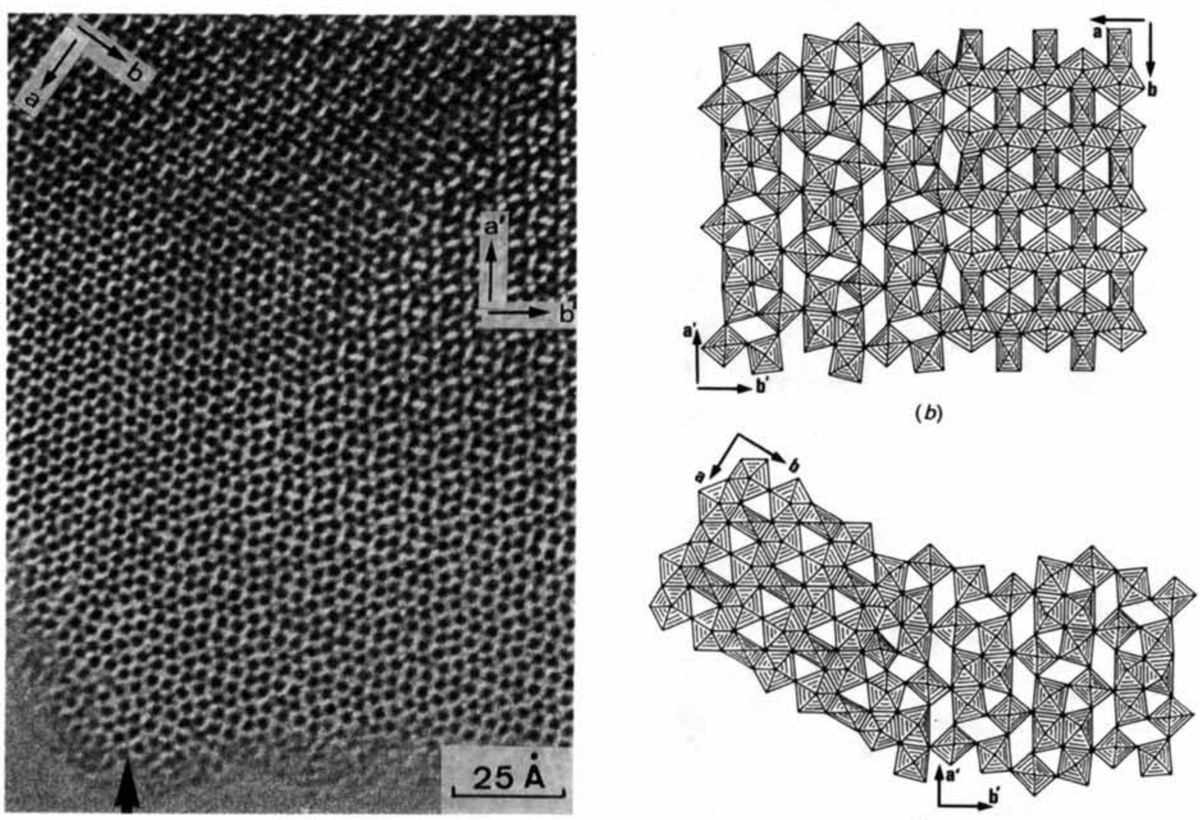

Fig. 4. HREM image showing intergrowth of W_3O_8(I) (left) and W_3O_8(II) (right). The unit-cell axes of W_3O_8(I) are marked **a**, **b** and those of W_3O_8(II) are marked **a**′, **b**′. (*b*) and (*c*) are idealized structure models: (*b*) corresponds to the region above the arrows in Fig. 1 and (*c*) corresponds to the intergrowth structure in the HREM image in (*a*).

models it is apparent that the two structures are closely related and can transform into each other by small atom displacements without change of stoichiometry.

Discussion

The two phases, both of composition W_3O_8 ($WO_{2.667}$), do not appear in the binary W–O system at ambient pressure. W_3O_8(I) has a structure of the U_3O_8 type (Andresen, 1958), which is denser than that of W_3O_8(II). The latter has a new type of structure, although some features are shared with other previously known tungsten oxides ({102} CS structures).

The relationship between the W_3O_8(II) structure and the {102} CS structure can be seen in Fig. 5. Both contain groups of four edge-sharing WO_6 octahedra and additional WO_6 octahedra connected by corner-sharing in different arrangements. In the W_3O_8(II) structure in Fig. 5(*a*) every second group of four edge-sharing octahedra appears in twin orientation and the groups are more densely packed than in the {102} CS structures, represented by the M_8O_{23} member of the homologous series in Fig. 5(*b*). The groups of edge-sharing octahedra account for the deficiency in oxygen compared to the parent WO_3 stoichiometry. Both structure types can theoretically be considered as formed by oxygen removal from WO_3. Hypothetical models will be discussed elsewhere.

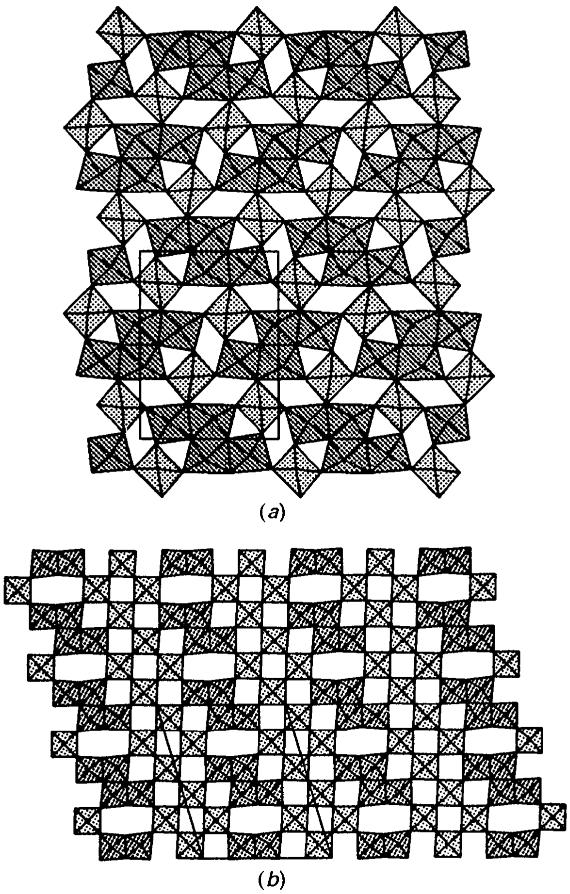

(*a*) (*b*)

Fig. 5. Crystal structures of (*a*) W_3O_8(II) and (*b*) M_8O_{23}, representative of the {102} CS structures.

The structure of W_3O_8(I) is denser than that of W_3O_8(II). This is indicated by the volume of the unit cell divided by the number of O atoms, which is 15.81 for W_3O_8(I) and 17.64 Å^3 for W_3O_8(II). The first value is even less than that of 16.53 Å^3 calculated for the ambient pressure WO_2 structure. Experiments to anneal the specimen at ambient pressure showed that at $T > 573$ K W_3O_8(I) transformed into the W_3O_8(II) phase which later, at $T > 1073$ K, decomposed into the $W_{18}O_{49}$ and WO_2 phases.

The W_3O_8(I) phase has also been observed in samples prepared from stoichiometric mixtures of W and WO_3 heated at high temperature in combination with high pressure. It does not seem very likely that carbon from the graphite container material promotes the formation of the W_3O_8 structures. The preparation methods and the phase analysis of the system will be presented in a joint forthcoming article.

We wish to thank Professor A. Magnéli for stimulating discussions and valuable comments on the manuscript. This study has partly been performed within a program for Swedish–Russian joint research projects. Financial support from the Royal Swedish Academy of Sciences and from the Swedish Natural Science Research Council is gratefully acknowledged.

References

Andresen, A. F. (1958). *Acta Cryst.* **11**, 612–614.

Barabanenkov, Yu. A., Valkovskii, M. D., Zakharov, N. D., Zibrov, I. P., Popov, A. I. & Filonenko, V. P. (1992). *Z. Neorg. Khim.* **37**, 19–25.

Barabanenkov, Yu. A., Zakharov, N. D., Zibrov, I. P., Filonenko, V. P. & Werner, P. (1992). *Kristallografiya*, **37**, 617–625.

Hovmöller, S. (1992). *Ultramicroscopy*, **41**, 121–135.

Jahnberg, L. (1971). *Chem. Commun. Univ. Stockholm*, **13**, 1–42.

Loopstra, B. O. (1964). *Acta Cryst.* **17**, 651–654.

Magnéli, A. (1949). *Ark. Kemi*, **1**, 223–230.

Magnéli, A. (1950). *Ark. Kemi*, **1**, 513–523.

Magnéli, A. (1953). *Acta Cryst.* **6**, 495–500.

O'Keefe, M. A., Buseck, P. R. & Iijima, S. (1978). *Nature (London)*, **274**, 322–324.

Sahle, W. (1983). *Chem. Commun. Univ. Stockholm*, **4**, 1–53.

Sundberg, M. (1976). *Acta Cryst.* **B32**, 2144–2149.

SUNDBERG, M. (1978–1979). *Chem. Scr.* **14**, 161–166.
SUNDBERG, M. (1981). *Chem. Commun. Univ. Stockholm*, **5**, 1–53.
SUNDBERG, M. & TILLEY, R. J. D. (1974). *J. Solid State Chem.* **11**, 150–160.
SUNDBERG, M., WERNER, P.-E., ZIBROV, I. P. & LOUËR, D. (1994). In preparation.
TILLEY, R. J. D. (1970). *Mater. Res. Bull.* **5**, 813–824.
TILLEY, R. J. D. (1978–1979). *Chem. Scr.* **14**, 147–159.

Acta Cryst. (1993). **B49**, 958–967

Proton Ordering in the Peierls-Distorted Hydrogen Molybdenum Bronze $H_{0.33}MoO_3$: Structure and Physical Properties

BY STEFAN ADAMS,* KARL-HEINZ EHSES AND JOACHIM SPILKER

Fachbereich Kristallographie der Universität des Saarlandes, D-66041 Saarbrücken, Germany

(*Received 3 March* 1993; *accepted* 21 *June* 1993)

Abstract

The intercalation of hydrogen into the layered structure of MoO_3 produces four hydrogen molybdenum bronze phases H_xMoO_3 ($0 < x < 2$). The correlation between the structure and the physical properties of these low-dimensional conductors has been investigated by X-ray diffraction and conductivity measurements. Powder diffraction studies revealed phase transitions as a function of temperature and hydrogen content. A new proton-distribution model describes the lattice distortions resulting from the intercalation in the whole composition range. Superstructure reflections were detected in precession photographs of single crystals of the phases I ($x \simeq 0.3$) and III ($x \simeq 1.6$). A single-crystal structure determination was performed for $H_{0.33}MoO_3$, which exhibits a $3a \times 6c$ superstructure at ambient temperature. Structural and experimental data for this particular composition are: $P^{2}_{b}{}^{1}11$, $a = 11.70$ (1), $b = 14.070$ (5), $c = 22.40$ (2) Å, $\alpha = 90.0$ (1)°, $V = 3687$ (8) Å^3, $Z = 72$, $D_x = 4.68$ (1) Mg m^{-3}, λ(Mo $K\alpha$) = 0.7107 Å, $\mu = 0.593$ cm^{-1}, $F(000) = 4622.6$, $R(F) = 0.10$ for 1223 unique reflections. Valence-sum calculations revealed that all the protons of $H_{0.33}MoO_3$ are located in periodically arranged 6-(OH)-clusters. The long-range proton ordering breaks down at $T_c = 380$ K giving rise to a second-order phase transition. The identification of this transition as a Peierls distortion explains many properties of phase I: conductivity measurements show a metal to non-metal transition at T_c with an unusual temperature dependence of σ in the ordered phase. The multiplication of the unit cell along the c direction as well as T_c depend on the hydrogen content x. The critical exponent of the order parameter $\beta = 0.36$ is compatible with an incommensurate superstructure. Fröhlich conductivity as a result of charge-density-wave depinning is observed in field-dependent conductivity measurements.

* Present address: Max-Planck-Institut für Festkörperforschung, Heisenbergstrasse 1, D-70569 Stuttgart.

Introduction

The hydrogen molybdenum bronzes H_xMoO_3 ($0 < x < 2$) have been the subject of intense studies throughout the last 20 years. Technical interest in the deeply coloured, conducting intercalate phases was raised by a great number of possible applications (*e.g.* hydrogen-transfer catalysts, electrochromic displays, fuel cells, hydrogen storage, gas sensors).

Scientific investigations of the molybdenum bronzes focused on the electronic and ionic charge transport in these mixed low-dimensional conductors. An understanding of the correlations between the structural modifications by intercalation and the distinct changes in the physical properties remained rather limited.

The layered structure of MoO_3 permits the intercalation of protons onto two different types of sites. Protons can occupy places in the van der Waals gaps between the octahedra layers as well as intralayer sites on zigzag chains along the c direction (Fig. 1). Among the four resulting bronze phases, three exist over wide composition ranges (phase I, $0.23 < x < 0.40$; phase II, $0.85 < x < 1.04$; phase III, $1.55 < x < 1.72$). Phase IV, in contrast, proved to be the stoichiometric compound H_2MoO_3 (Birtill & Dickens, 1978).

Powder data

Experimental

Powder samples of phase III were prepared by electrochemical intercalation of hydrogen into

ISSN 0108-7681